J Mol Model (2019) 25: 149
https://doi.org/10.1007/s00894-019-4017-4

ORIGINAL PAPER

Polaron properties in 2D organic molecular crystals: directional dependence of non-local electron–phonon coupling

Marcelo Lopes Pereira Junior[1] · Rafael Timóteo de Sousa Júnior[2] · Bernhard Georg Enders Neto[3] · Geraldo Magela e Silva[1] · Luiz Antonio Ribeiro Junior[4]

Received: 31 January 2019 / Accepted: 29 March 2019 / Published online: 7 May 2019

Abstract
In organic molecular crystals, the polaronic hopping model for the charge transport assumes that the carrier lies at one or a small number of molecules. Such a kind of localization suffers the influence of the non-local electron–phonon (e–ph) interactions associated with intermolecular lattice vibrations. Here, we developed a model Hamiltonian for numerically describing the role played by the intermolecular e–ph interactions on the stationary and dynamical properties of polarons in a two-dimensional array of molecules. We allow three types of electron hopping mechanisms and, consequently, for the nonlocal e–ph interactions: horizontal, vertical, and diagonal. Remarkably, our findings show that the stable polarons are not formed for isotropic arrangements of the intermolecular transfer integrals, regardless of the strengths of the e–ph interactions. Interestingly, the diagonal channel for the e–ph interactions changes the transport mechanism by sharing the polaronic charge between parallel molecular lines in a breather-like mode.

Keywords Holstein–Peierls model · Polaron · Electron–phonon coupling · Charge transport · Organic semiconductors

Introduction

Organic molecular crystals are attractive due to their intrinsic physical-chemical properties, which are substantially different from the ones exhibited by conventional solids such as ionic and covalent crystals [1]. The generally weak intermolecular van der Waals interactions as well as the interplay between intra and intermolecular degrees of freedom, aggregate to these materials unique properties that are desired to the manufacturing of optoelectronic devices.

Recently, relevant theoretical studies have drawn attention to the importance of the symmetry effects on electron–phonon (e–ph) coupling mechanism in organic semiconductors [1–3]. By using a tight-binding approach, these works provide a good understanding of how the local and nonlocal e–ph coupling channels affect the electronic and charge transport properties. Although these studies elucidate the role played by these channels in some features of organic crystalline semiconductors, to further understand the polaron properties, additional investigations are required. Importantly, the relative orientation of molecules, associated with nonlocal e–ph interactions, that, in turn, modulate the intermolecular lattice vibrations, is a fundamental issue that remains not well understood.

Herein, by employing a two-dimensional version of the Holstein–Peierls Hamiltonian [4, 5], we present a tight-binding description that underlines the impact of the relative molecular orientation—as a function of the symmetry of the nonlocal electron–phonon coupling mechanism—on the static and dynamical properties of polarons in crystalline

This paper belongs to Topical Collection VII Symposium on Electronic Structure and Molecular Dynamics – VII SeedMol

✉ Marcelo Lopes Pereira Junior
marcelolpjunior@gmail.com

Geraldo Magela e Silva
magela@unb.br

Luiz Antonio Ribeiro Junior
ribeirojr@unb.br

[1] Institute of Physics, University of Brasília, Brasília, 70910-900, Brasília, Brazil

[2] Department of Electrical Engineering, University of Brasília, CP04455, Brasília, 70919-970, Brazil

[3] University of Brasília, PPG-CIMA, Campus Planaltina, 73345-010, Brasília, DF, Brazil

[4] International Center for Condensed Matter Physics, University of Brasília, PO Box 04531, 70.919-970, Brasília, DF, Brazil

organic semiconductors. Our computational protocol defines a molecular array, in which three types of electron hopping is allowed: horizontal, vertical, and diagonal. The nonlocal e–ph interactions follow the scheme used for the intramolecular electronic coupling mechanism.

Methodology

The model tight-binding Hamiltonian developed here takes into account both intramolecular (Holstein) and intermolecular (Peierls) interactions for a two-dimensional array of molecules of (20 × 20 sites) with periodic boundary conditions. In our system, each lattice site represents a (i, j) molecule of the molecular array, as depicted in Fig. 1. The indexes i and j label the molecular "rows" (x-direction) and "columns" (y-direction), respectively. In this way, the overall model Hamiltonian assumes the following form

$$H = H_{\text{elec,intra}} + H_{\text{elec,inter}} + H_{\text{latt,intra}} + H_{\text{latt,inter}}, \tag{1}$$

where $H_{\text{elec,intra}}$ and $H_{\text{elec,inter}}$ denote the intra and intermolecular electronic contributions whereas $H_{\text{latt,intra}}$ and $H_{\text{latt,inter}}$ describe the intra and intermolecular lattice contributions, respectively.

The intramolecular electronic contribution is

$$H_{\text{elec, intra}} = \sum_{i,j} \alpha_1 u_{i,j} \hat{c}^{\dagger}_{i,j} \hat{c}_{i,j}. \tag{2}$$

In this equation, $u_{i,j}$ denotes the internal vibrational phonon mode for a (i, j) molecule, which interacts with the electronic degree of freedom by means of a intramolecular

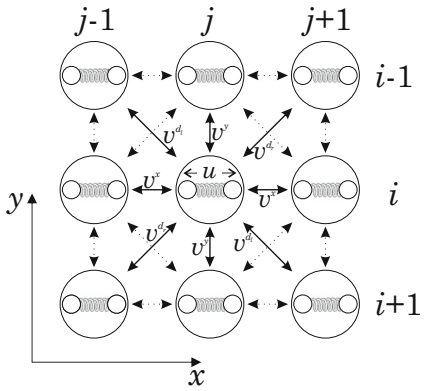

Fig. 1 Schematic representation of the two-dimensional array of molecules considered here. In this representation, v^x and v^y denote the relative displacement of a (i, j) molecule, from its equilibrium, in the x- and y-direction, respectively, whereas v^{d_r} and v^{d_l} state the relative displacement of a molecule in the right and left diagonal directions, respectively

e–ph coupling constant α_1. The operator $\hat{c}^{\dagger}_{i,j}\left(\hat{c}_{i,j}\right)$ creates (annihilates) a carrier at the (i, j)-th site of the lattice. The intermolecular electronic degree of freedom, in turn, can be placed in the form

$$\begin{aligned} H_{\text{elec, inter}} = & \sum_{i,j}\left(J^{x}_{i,j+1;\,i,j}\hat{c}^{\dagger}_{i,j+1}\hat{c}_{i,j} + \text{H.C.}\right) \\ & + \sum_{i,j}\left(J^{y}_{i+1,j;\,i,j}\hat{c}^{\dagger}_{i+1,j}\hat{c}_{i,j} + \text{H.C.}\right) \\ & + \sum_{i,j}\left(J^{d_r}_{i+1,j-1;\,i,j}\hat{c}^{\dagger}_{i+1,j-1}\hat{c}_{i,j} + \text{H.C.}\right) \\ & + \sum_{i,j}\left(J^{d_l}_{i+1,j+1;\,i,j}\hat{c}^{\dagger}_{i+1,j+1}\hat{c}_{i,j} + \text{H.C.}\right). \end{aligned} \tag{3}$$

$J^{x}_{i,j;\,i',j'}$, $J^{y}_{i,j;\,i',j'}$, $J^{d_r}_{i,j;\,i',j'}$, and $J^{d_l}_{i,j;\,i',j'}$ denote the intermolecular transfer integrals between next-neighboring molecules (i, j) and (i', j') in the horizontal x, vertical y, and right (d_r) and left (d_l) diagonals, respectively. These electronic transfer integrals are given by

$$J^{x}_{i,j+1;\,i,j} = J^{x}_{0} - \alpha^{x}_{2}\left(v^{x}_{i,j+1} - v^{x}_{i,j}\right), \tag{4}$$

$$J^{y}_{i+1,j;\,i,j} = J^{y}_{0} - \alpha^{y}_{2}\left(v^{y}_{i+1,j} - v^{y}_{i,j}\right), \tag{5}$$

$$J^{d_r}_{i+1,j-1;\,i,j} = J^{d_r}_{0} - \alpha^{d_r}_{2}\left(v^{d_r}_{i+1,j-1} - v^{d_r}_{i,j}\right), \tag{6}$$

and

$$J^{d_l}_{i+1,j+1;\,i,j} = J^{d_l}_{0} - \alpha^{d_l}_{2}\left(v^{d_l}_{i+1,j+1} - v^{d_l}_{i,j}\right). \tag{7}$$

In this set of equations, $v^{x}_{i,j}$, $v^{y}_{i,j}$, $v^{d_l}_{i,j}$ and $v^{d_r}_{i,j}$ describe the intermolecular displacements of a (i, j) molecule from its equilibrium in the x, y, left (d_l) and right (d_r) diagonals, respectively. J_0 denotes the transfer integral values for a system where the lattice sites are equally spaced. α_2^{x,y,d_l,d_r} is the intermolecular e–ph coupling constant that considers the three distinct coupling of the intermolecular lattice vibrations.

The lattice treatment used here consists in describing the phonons using two distinct harmonic oscillators to account the intra and intermolecular lattice vibrations separately. Such an approach yields the following contributions to the model Hamiltonian:

$$H_{\text{latt, intra}} = \frac{1}{2}K_1\sum_{i,j}\left(u_{i,j}\right)^2 + \frac{1}{2}M_1\left(\dot{u}_{i,j}\right)^2 \tag{8}$$

and

$$
\begin{aligned}
H_{\text{latt, inter}} = & \frac{1}{2}K_2\sum_{i,j}\left(v^x_{i,j+1}-v^x_{i,j}\right)^2 \\
& +\frac{1}{2}K_2\sum_{i,j}\left(v^y_{i+1,j}-v^y_{i,j}\right)^2 \\
& +\frac{1}{2}K_2\sum_{i,j}\left(v^{d_l}_{i+1,j-1}-v^{d_l}_{i,j}\right)^2 \\
& +\frac{1}{2}K_2\sum_{i,j}\left(v^{d_r}_{i+1,j+1}-v^{d_r}_{i,j}\right)^2 \\
& +\frac{1}{2}M_2\sum_{i,j}\left(\left(\dot{v}^x_{i,j}\right)^2+\left(\dot{v}^y_{i,j}\right)^2\right. \\
& \left.+\left(\dot{v}^{d_r}_{i,j}\right)^2+\left(\dot{v}^{d_l}_{i,j}\right)^2\right). \qquad (9)
\end{aligned}
$$

In the equations above, the force constants K_1 and K_2 and also the masses M_1 and M_2 refer to the intra and intermolecular oscillators, respectively.

The present work investigates the impact of orientation effects on nonlocal e–ph coupling and their consequences on the static and dynamic properties of polarons at organic crystalline semiconductors. To do so is necessary to prepare a convenient set of parameters that can address the essential physics behind the polaron properties in the systems. The model parameters considered here lie in the range of those widely used to reflect the electronic and vibrational properties of oligoacene-like crystals, such as pentacene [6], anthracene [7], and rubrene [8]. In this way, we adopt the following set of parameters: $J_0^x = J_0^y = 50$ meV, $\alpha_1 = 1.8$ eV/Å, $\alpha_2^x = \alpha_2^y = 0.4$ eV/Å, $K_1 = 14$ eV/Å^2, $K_2 = 0.9$ eV/Å^2, $M_1 = 2.88\times10^{10}$ eV(as/Å)^2, and $M_2 = 5.76\times10^{10}$ eV(as/Å)^2. The diagonal parameters $J_0^{d_r}$, $J_0^{d_l}$, $\alpha_2^{d_r}$, and $\alpha_2^{d_l}$ lie in the range of [0-50] meV (for the transfer integrals) and [0-0.4] eV/Å(for the e–ph coupling terms), respectively. Such a range of values yields outcomes that allow to better understand the interplay between the different channels for the e–ph interactions. It is worth mentioning that the force constants used here derive from experimental frequencies [9, 10].

All the calculations performed here obtain optimized geometries for the lattice containing an extra positive charge. To achieve a self-consistent ground state geometry for a particular set of parameters, we use the Resilient backPROPagation algorithm (RPROP) [11]. This ground state geometry is the starting point to investigating the static and dynamical properties of the polarons. Regarding the polaron dynamics, the system evolves in time by using an Ehrenfest Molecular Dynamics method, i.e., an approach where the temporal evolution of the electronic and lattice degrees of freedom occurs in a coupled fashion and governed by the time-dependent Schrödinger and Euler–Lagrange equations, respectively [12].

Results

Having presented the details about our approach, we now move to the discussions of the results. We begin by discussing the impact of the interplay between the intermolecular e–ph mechanisms on the static properties associated with the presence of a polaron in the lattice. To obtain an overall physical insight about these properties, here we use two measurements: the polaron formation energy (E_P) and the inverse participation ration (IPR). The E_P consists of the amount of energy required for the system to form a polaron, i.e., the energy difference between the neutral ground state and the charged lattice (an additional electron or hole). For stable polarons, $E_p > 0$. If $E_p \gg J_0^x$ (or J_0^y), ground state geometry calculations yield a charge carrier that is essentially localized in a single molecule. In this way, the Holstein model prevails, and the charge carrier description follows the small polaron picture [13, 14]. In contrast, if $E_p \sim J_0^x$ (or J_0^y), the molecular charge extends over the next-neighboring sites concerning a central unit and the charge carriers yielded, in this case, are denoted as large polarons (Fröhlich model) [4].

The IPR concept, in turn, characterizes the polaron localization, i.e., this quantity is a measure of how many sites share the extra charge. For IPR values between 0.4 and 0.8, the charge is usually shared by five molecules yielding a large polaron solution. This kind of charge carrier is the fundamental structure behind the charge transport mechanism when it comes to organic crystalline semiconductors [1]. Conversely, IPR values greater than 0.8 yield polaron solutions in which the charge lies, solely, at one molecule (small polarons). Through the IPR calculation, we can derive an important electronic parameter when organic materials are considered: the lattice reorganization energy (λ). This parameter accounts for the energy cost in displacing the molecules, from their equilibrium position, in the presence of an additional charge. Here, λ is derived according to the expression $\lambda = \lambda_0/\text{IPR}$, where λ_0 is the reorganization energy for the removal of an electron or hole from a single molecule. We adopt 59 meV for λ_0, according to the reference [15].

With the derivation of λ and E_P in mind, we now discuss the results presented in Fig. 2. Figure 2a depicts the lattice reorganization energy as a function of the interplay between the intermolecular e–ph couplings and the transfer integrals for all degrees of freedom. The performed calculations consider a set of parameters in which the

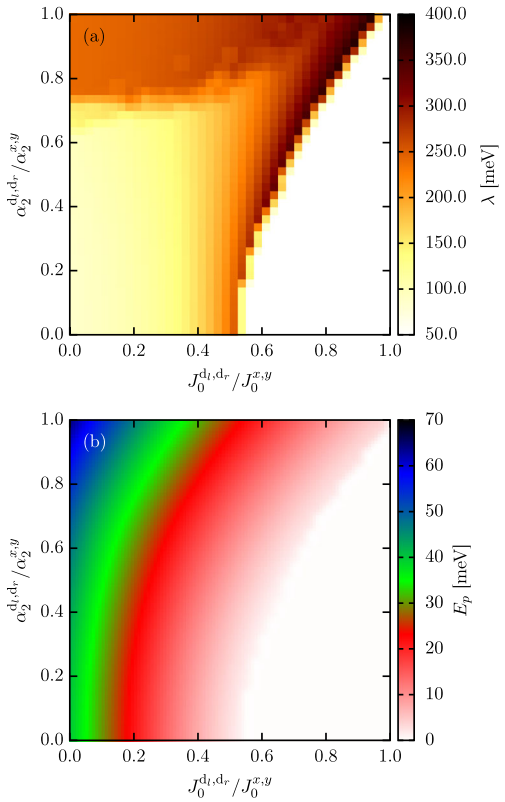

Fig. 2 The phase diagram for the **a** reorganization energy (λ) and **b** the polaron formation energy (E_P) yielded according the interplay between the intermolecular e–ph couplings and the transfer integrals for all degrees of freedom

e–ph couplings and the transfer integrals for the diagonal directions were systematically varied from 0-0.5 eV/Åand 0-50 meV, respectively. The strengths for $\alpha_2^{x,y}$ and $J_0^{x,y}$ were settled as 0.5 eV/Åand 50 meV, respectively. In this way, one can see from Fig. 2a that there are two distinct and well-defined dominant regions for the λ values. The white region denotes reorganization energy values (about 50 meV) for which the parameters yield pristine lattices (free of polarons). According to our calculations, the minimum reorganization energy required to realize the formation of stable polarons is about 59 meV, which agrees with the reorganization energy obtained for pentacene lattices [15]. These forbidden parameter relationships for the polaron formation are obtained outcomes when all the strengths of the intermolecular transfer integrals assume the critical value, i.e., 50 meV. In these cases, the molecular charge is over-delocalized in such a way that the lattice is not sufficiently deformed to couple the extra charge in a self-interacting state that can form a stable polaron.

Conversely, for the interplay between parameters where the intermolecular e–ph couplings of all directions assume the critical value, i.e., 0.5 eV/Å, the ground state geometry calculations always yield λ values greater then 60 meV (in other words, stable polarons are formed), excluding the case in which $J_0^{d_l,d_r}/J_0^{x,y} = 1$. Since the strength of the e–ph couplings is increased, the degree for the lattice deformation in the region where the charge is localized increase dramatically. This higher degree of distortion is responsible for coupling the charge and the lattice in a stronger fashion, which substantially raises the reorganization energy due to the higher molecular displacements. We can state that the parameter space represented by the light-yellow region in Fig. 2a is of particular interest since the λ values lie in the range of 60–150 meV, which are values usually reported in the literature for oligoacene-like crystals [1, 15]. In this context, the orange and dark regions in the panel are less of interest, since the reorganization energies calculated are higher than 200 meV. Importantly, from these results, it is possible to determine a physical parameter space in which stable polarons are formed, in the context of the model Holstein–Peierls Hamiltonian defined above. Moreover, we have studied the impact of the interplay between intra and intermolecular e–ph coupling strengths on the polaron delocalization very recently [16]. In that study, four quasiparticle solutions were found: free-like electrons, metastable polarons, and small and large polarons. The latter governs the charge transport in organic crystalline semiconductors. In Fig. 2, the stable charge carriers yielded are large polarons.

A complementary description of the static polaron properties can be provided by analyzing the impact of the interplay between the intermolecular (Peierls) parameters on the polaron formation energy. Figure 2b presents the E_p using the same numerical procedure employed for the case showed in Fig. 2a. Here, we can still observe the presence of two distinct regions. Moreover, one can note that the white regions in Fig. 2a and b are coincident. Consistently, for the parameter spaces where the reorganization energy assumes a small value the polaron formation is forbidden and, consequently, $E_p = 0$ as can be seen in Fig. 2b. For the second well-established region presented in Fig. 2b, the blue region, the interplay between the intermolecular parameters yield polaron formation energies lying in the range 30–70 meV. These values are typical when it comes to oligoacene-like crystals [1, 15]. In this way, any set of parameters within the blue region describes stable polarons and should be considered in combination with the results for λ, once some of these parameters are undesirable because they can yield unrealistic λ values, the orange and dark regions in Fig. 2a.

Now we turn to the results obtained for the lattice ground state geometries in the presence of a stable polaron. This analysis helps to realize the interdependence between charge and lattice deformations, i.e., the phonon system. In this way, Fig. 3 shows the molecular charge distribution as well as the lattice bond-length changes—which are induced by the presence of an additional charge—considering the

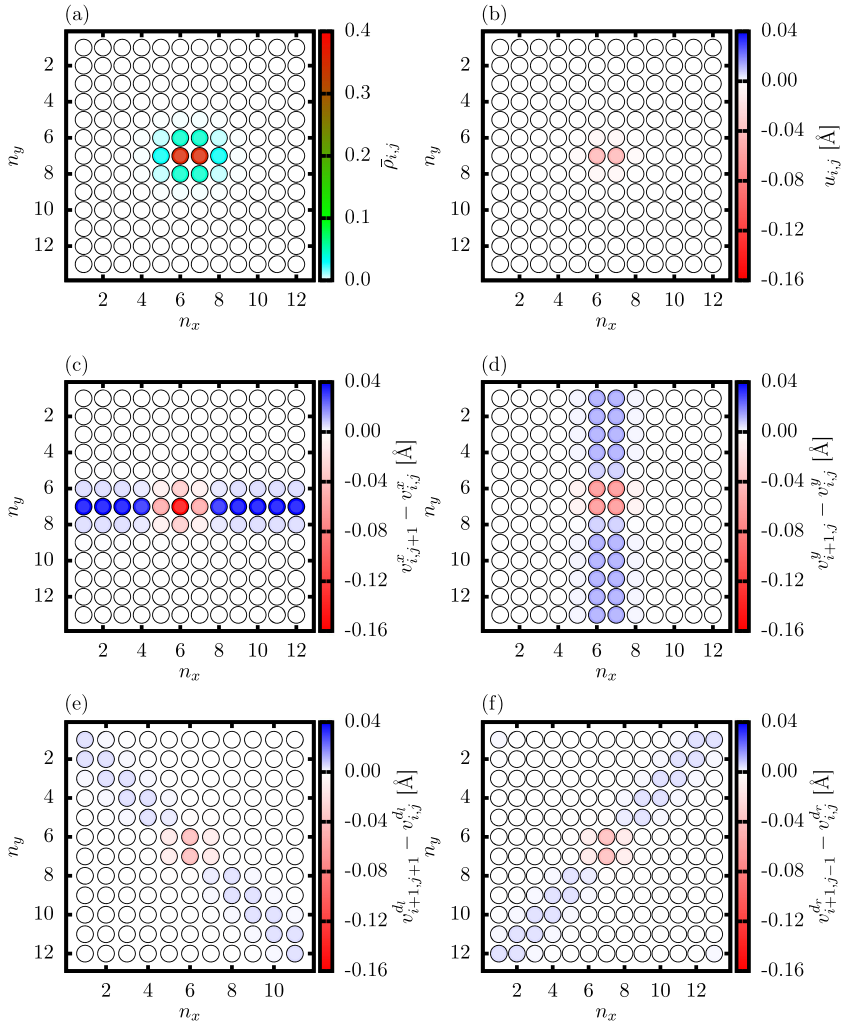

Fig. 3 Molecular charge distribution and lattice configuration for the case where a stable polaron is formed. **a** Molecular charge density, **b** intramolecular displacements ($u_{i,j}$) and intermolecular bond-lengths in the (**c**) horizontal ($v^x_{i,j+1} - v^x_{i,j}$), **d** vertical ($v^y_{i+1,j} - v^y_{i,j}$), **e** left-diagonal ($v^{d_l}_{i+1,j+1} - v^{d_l}_{i,j}$), and **f** right-diagonal ($v^{d_r}_{i+1,j-1} - v^{d_r}_{i,j}$) directions

different degrees of freedom for the e–ph coupling included in our model Hamiltonian. This signatures for the charge and lattice configurations denote the presence of a stable polaron. Here, $J^x_0 = 50$ meV, $J^y_0 = 30$ meV, and $J^{d_l}_0 = J^{d_r}_0 = 10$ meV. For the e–ph coupling we adopt $\alpha^x_2 = 0.5$ eV/Å, $\alpha^y_2 = 0.3$ eV/Å, and $\alpha^{d_l}_2 = \alpha^{d_r}_2 = 0.25$ eV/Å. The anisotropy in the values for J^x_0 and J^y_0 is a necessary condition to realize the polaron dynamics, in the context of the Holstein–Peierls model, as reported in the reference [17, 18]. J^{d_l,d_r}_0 were settled according the discussions for the Fig. 2. It is worthwhile to mention that the molecular charge density ($\bar{\rho}_{i,j}$) follows the expression presented in reference [19].

In Fig. 3, each circle represents a site of the lattice. The white circles denote the absence of charge and distortions for the molecules. n_x and n_y count the number of columns and lines for the molecular array, respectively. The depicted system is a 13 × 13 lattice. In some panels, n_x is adjusted to present the results better. In this sense, Fig. 3a depicts the molecular charge configuration. One can note that part of the additional charge lies at two molecules (red circles) and the rest spread over next-neighboring ones in the horizontal, vertical, and diagonal directions. Such a configuration for the charge density localization denotes a large polaron structure with a two-dimensional nature. Figure 3b shows the intramolecular distortions $u_{i,j}$ for the molecules in the molecular array. From this figure, one can rapidly note that $u_{i,j}$ present negative values for the lattice sites where the charge is localized. The sites with a higher concentration of charge present, consequently, higher degrees of deformation (red circles). These deformations denote compressions in the molecular structure due to the presence of charge. Therefore, these intramolecular responses are the signature of the self-interacting state involving charge and lattice, which is mediated by the e–ph coupling mechanism.

The system's trend in localizing the extra charge has, of course, a pronounced impact in the intermolecular arrangement of the lattice. Figure 3c–f present the intermolecular bond lengths in the horizontal ($v^x_{i,j+1} - v^x_{i,j}$), vertical ($v^y_{i+1,j} - v^y_{i,j}$), left-diagonal ($v^{d_l}_{i+1,j+1} - v^{d_l}_{i,j}$), and

right-diagonal ($v^{d_r}_{i+1,j-1} - v^{d_r}_{i,j}$), respectively. In Fig. 3c, we can see that the horizontal deformations extend over a central line, with a high degree of distortion, and over lines above and below regarding the central one, with a smaller degree of distortion. In the region where a considerable part of the charge is localized, the bond lengths in x-direction show a compression (red circles), which are also noted to be present in the next-neighboring sites. These compressions are followed by lattice expansions (blue circles) through the molecular lines for which, at least, one red circle is present. Such a configuration for the bond lengths is a shrinking-like effect that moves next-neighboring molecules towards the central unities that contain the charge.

Similarly, there is a bond-length pattern distributed along the y-direction, as depicted in Fig. 3d. The bond lengths in the y-direction are oriented, in a symmetric fashion, according to the sites that contain the charge. Through the color scheme, we can note that the distortions for the molecule positions in the y-direction are smaller than the ones in the x-direction. This behavior occurs due to the smaller strengths adopted for the e–ph coupling and the transfer integral in the y-direction. The lattice deformations for both diagonals can be described using the same arguments above. Note that the bond-length values in these cases are the smaller ones. Again, these low amplitudes for the displacements of the molecules are related to the values adopted for the e–ph coupling and the transfer integrals in the diagonal directions.

Finally, we turn to the discussions for the polaron dynamics. Figure 4 shows the time evolution for the mean charge density for the central line $i = 10$, where the additional charge is initially placed, and for its parallel lines $i = 9$ (bellow) and $i = 11$ (above). The dynamics occurs over 3 ps. Here, the two-dimensional nature of the polaron localization takes place. In the central line, we can note red and yellow regions, which denote sites with a high concentration of charge. Moreover, one can note that the parallel lines contain blue regions denoting a small concentration of charge. The mechanism for the polaron motion can be understood as follows: (I) the polaron is initially lying in line 10 (red and green regions) by sharing a small portion of its charge among parallel lines; (II) after approximately 400 fs, the charge moves to just a central line, which can be noted by the white regions in lines 9, and; (III) soon afterward, the polaronic charge assumes its initial configuration. This mechanism for the polaron transport repeats during the simulation time in a breather-like mode with a period of about 400 fs. Importantly, this signature for the polaron dynamics is not present in the absence of the diagonal channel for the e–ph coupling mechanism [19]. Note that, in the absence of the diagonal channel for the e–ph coupling, the charge transport mechanism presents the same behavior for the motion of the net charges localized in the main and the parallel molecular lines [19]. When the diagonal e–ph coupling is considered, a breather-like mode to the charge localization with a period of about 400 fs takes place. In this trend of motion, the charge localizes by oscillating in time into one and three molecular lines as shown in Fig. 4.

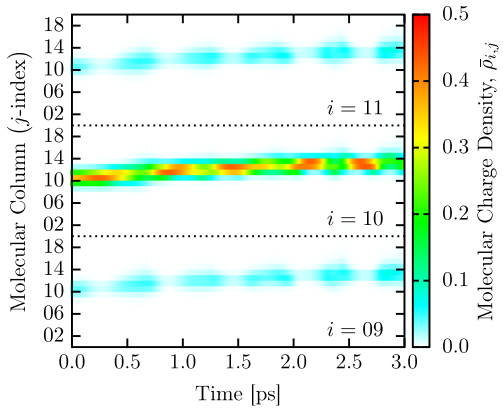

Fig. 4 Polaron dynamics in a molecular array of 20 × 20 sites. For the sake of clarity, just the central line as well as its parallel ones are depicted

Conclusions

In conclusion, we have studied the static and dynamical properties of polarons organic molecular crystals by developing a model Hamiltonian that takes into account different orientations for the nonlocal electron–phonon coupling mechanism. These orientations are implemented by including in different Hamiltonian types for the electron hopping mechanism and the nonlocal e–ph interactions: horizontal, vertical, and diagonal. The outcomes have shown that there are two distinct regimes concerning the polaron formation. In one of them, the high strengths of the intermolecular transfer integrals inhibit the formation of polarons by over-delocalizing the molecular charge. Importantly, the results have shown that the stable polarons are not formed for isotropic arrangements of the intermolecular transfer integrals, regardless of the strengths of the e–ph interactions. Conversely, for the other set of parameters, large and small polarons are formed by presenting lattice reorganization energies that agree with theoretical results in the literature [15]. Regarding the polaron dynamics, the diagonal channel for the e–ph interactions leads to a breather-like mode for the charge motion. This mode is not observed in the absence of diagonal interactions.

Acknowledgments The authors gratefully acknowledge the financial support from Brazilian Research Councils CNPq, CAPES, and FAPDF and CENAPAD-SP for providing the computational facilities.

This research work has the support of the Brazilian Ministry of Planning, Development and Management (Grants 005/2016 DIPLA – Planning and Management Directorate, and 11/2016 SEST – State-owned Federal Companies Secretariat) and the DPGU – Brazilian Union Public Defender (Grant 066/2016). L.A.R.J. and G.M.S. gratefully acknowledge the financial support from FAP-DF grants 0193.001.511/2017 and 0193.001.766/2017, respectively.

References

1. Coropceanu V, Cornil J, da Silva Filho DA, Olivier Y, Silbey R, Brédas JL (2007) Chem Rev 107:926. https://doi.org/10.1021/cr050140x
2. Li Y, Coropceanu V, Brédas JL (2013) J Chem Phys 138:204713. https://doi.org/10.1063/1.4807886
3. Li Y, Yi Y, Coropceanu V, Brédas JL (2012) Phys Rev B 85:245201. https://doi.org/10.1103/PhysRevB.85.245201
4. Stafström S (2010) Chem Soc Rev 39:2484. https://doi.org/10.1039/B909058B
5. Troisi A (2011) Chem Soc Rev 40:2347. https://doi.org/10.1039/C0CS00198H
6. Nelson SF, Lin YY, Gundlach DJ, Jackson TN (1998) Appl Phys Lett 72:1854. https://doi.org/10.1063/1.121205
7. Castet F, Aurel P, Fritsch A, Ducasse L, Liotard D, Linares M, Cornil J, Beljonne D (2008) Phys Rev B 77:115210. https://doi.org/10.1103/PhysRevB.77.115210
8. Podzorov V, Gershenson ME, Kloc C, Bucher E (2004) Appl Phys Lett 84:3301. https://doi.org/10.1063/1.1723695
9. Sanchez-Carrera RS, Paramonov P, Day GM, Coropceanu V, Brédas JL (2010) J Amer Chem Soc 132:14437. https://doi.org/10.1021/ja1040732
10. Sanchez-Carrera RS, Coropceanu V, da Silva Filho DA, Friedlein R, Osikowicz W, Murdey R, Suess C, Salaneck WR, Brédas JL (2006) J Phys Chem B 110:18904. https://doi.org/10.1021/jp057462p
11. Riedmiller M, Braun H (1993) Proc IEEE Inte Conf Neural Netw 1:586. https://doi.org/10.1109/ICNN.1993.298623
12. da Cunha WF, Junior LAR, Gargano R, e Silva GM (2014) Phys Chem Chem Phys 16:1707. https://doi.org/10.1039/c4cp02184c
13. Holstein T (1959) Ann Phys 8:325. https://doi.org/10.1016/0003-4916(59)90002-8
14. Holstein T (1959) Ann Phys 8:343. https://doi.org/10.1016/0003-4916(59)90003-X
15. Gruhn NE, da Silva Filho DA, Bill TG, Malagoli M, Coropceanu V, Kahn A, Brédas JL (2001) J Amer Chem Soc 124:7918. https://doi.org/10.1021/ja0175892
16. Pereira Junior ML, de Sousa Junior RT, e Silva GM, Ribeiro Junior LA (2019) Phys Chem Chem Phys 21:2727. https://doi.org/10.1039/C8CP06915H
17. Junior LAR, Stafström S (2015) Phys. Chem Chem Phys 17:8973. https://doi.org/10.1039/c4cp06028h
18. Junior LAR, Stafström S (2016) Phys Chem Chem Phys 18:1386. https://doi.org/10.1039/c5cp06577a
19. Mozafari E, Stafström S (2013) J Chem Phys 138:184104. https://doi.org/10.1063/1.4803691